Transportation Research Part D 98 (2021) 102971

Contents lists available at ScienceDirect

Transportation Research Part D

journal homepage: www.elsevier.com/locate/trd

Relationship between tyre cavity noise and road surface characteristics on low-noise pavements

Lara Ginevra Del Pizzo [a], Francesco Bianco [b], Antonino Moro [b], Gloria Schiaffino [c], Gaetano Licitra [d,e,*]

[a] University of Pisa, Physics Department, Largo Bruno Pontecorvo, 3, 56124 Pisa, Italy
[b] IPOOL srl, Via Antonio Cocchi, 7, 56121 Pisa, Italy
[c] Università Mediterranea di Reggio Calabria, Department of Information Engineering, Infrastructure and Sustainable Energy (DIIES), Via Graziella Loc. Feo di Vito, 89124 Reggio Calabria, Italy
[d] CNR - IPCF, Via Moruzzi, 1, 56124 Pisa, Italy
[e] ARPAT, Via Vittorio Veneto, 27, 56127 Pisa, Italy

ARTICLE INFO

Keywords:
Road traffic noise
Low-noise pavements
CPX method
Tyre cavity noise
Rubberized pavements

ABSTRACT

In this work, a protocol to study Tyre Cavity Noise (TCN) was developed. Using this new method, TCN was measured on 24 different road pavements, together tyre noise emission measured with the Close-Proximity (CPX) method and road texture measurements. The results were used to model the relationship between TCN and road surface parameters. The analysis shows that the Standard Reference Test Tyre's (SRTT) TCN is correlated to megatexture at low frequencies and that the correlation between TCN and outside noise emission is significant for frequencies lower than 1 kHz. The use of sensors placed inside the tyre for monitoring the acoustic performance of road pavements presents several advantages compared to the CPX method, such as a more compact design, lower cost and lower hazards both for the instrumentation and for other vehicles.

1. Introduction

Road Traffic Noise (RTN) represents one of the main cause of annoyance for people living close to roads both in urban or extra-urban environments. Indeed, high RTN levels are directly linked to sleep disturbances (Ouis, 2001; Muzet, 2007), cardiovascular diseases (Babisch et al., 2012), hypertension (Bluhm et al., 2007), myocardial infarction (Selander et al., 2009), and lower cognitive performance in children compared to quieter areas (Stansfeld et al., 2005). Therefore, RTN yields a significant impact on life quality close to roads (Botteldooren et al., 2011). Traffic noise arises from the composition of many sources, such as power train noise, noise caused by aerodynamic turbulence and tyre/road pavement interaction. For passenger vehicles, this last source becomes dominant at speeds higher that 30 km/h, while for heavier vehicles the influence of engine noise can be non-negligible up to 75 km/h (Sandberg and Ejsmont, 2002).

In order to reduce noise pollution deriving from the road infrastructure, the European Union has developed a series of guidelines summarised in the Green Public Procurement (GPP) published in 2008 and revised in 2016. The basic concept of GPP is to provide (Commission of the European Communities, 2008):

* Corresponding author.
E-mail addresses: lara.delpizzo@phd.unipi.it (L.G. Del Pizzo), francesco.bianco@i-pool.it (F. Bianco), antonino.moro@i-pool.it (A. Moro), gloria.schiaffino@unirc.it (G. Schiaffino), g.licitra@arpat.toscana.it (G. Licitra).

https://doi.org/10.1016/j.trd.2021.102971

Available online 22 July 2021

a process whereby public authorities seek to procure goods, services and works with a reduced environmental impact throughout their life-cycle when compared to goods, services and works with the same primary function that would otherwise be procured.

GPP also focuses on road construction and maintenance, and, in particular, sets guidelines for the development and monitoring of low-noise road surfaces (Garbarino et al., 2016), taking into account several factors; however, as far as noise is concerned, the GPP criteria provide limits to noise emission measured via Close Proximity (CPX) methods, prior to opening and at regular periods over the pavement's life cycle (Garbarino et al., 2016). Under this light, the development of low-noise surfaces becomes of paramount importance and monitoring their acoustic and superficial properties across time is crucial for monitoring the acoustic ageing processes.

One of the main advantages of the CPX protocol over other methods in monitoring the acoustic performance of road surfaces is the use of two or more microphones placed in close proximity to the tyre, whose aim is to measure the effect of pavement on traffic noise emission. While CPX measurements monitor near-field noise radiated outside the tyre, the use of a Tyre Cavity Microphone (TCM) offers a different acoustic perspective. This system provides a measurement of Tyre Cavity Noise (TCN), which is related to the near-field noise measured by the CPX method (Krauss and Gauterin, 2012) and is capable of distinguishing different road surfaces.

The use of TCM could represent an interesting innovation in monitoring the acoustic performance of road surfaces and their status, although, as far as noise emission is concerned, aerodynamic phenomena such as *air pumping*, and other amplification mechanisms like the *horn effect*, which highly influence outside emission, are not relevant inside the tyre cavity. Moreover, the setup of TCN measurements requires no equipment placed outside the vehicle and can thus be conducted in a smoother way compared to CPX measurements.

2. Our contribution

In this work, a new method to normalise TCN to a reference speed was used to perform measurements of TCN, together with CPX and road texture measurements, on 24 different road surfaces. The development of this method was brought about in order to correlate road surface properties and TCN. The analysis was carried out in one-third-octave band levels. Moreover, an algorithm capable of estimating the part of road texture actually in contact with the tyre was used. This algorithm, developed by Goubert and Sandberg (2018), was specifically designed for the Standard Reference Test Tyre (SRTT) used in CPX measurements. The result, called *enveloped texture*, was correlated to TCN. A linear model was developed for describing the relation between enveloped texture levels at 100 mm and noise at frequencies lower than 1 kHz in the reverberant field inside the tyre cavity. While TCN was connected by Pinay et al. (2018), to road surface synthetic indicators such as the Mean Profile Depth (MPD), no studies between TCN and road texture are available currently.

In addition, a qualitative study of the link between TCN and CPX noise was also performed. Usually, the results show again that low frequency TCN and CPX noise are correlated, despite the two quantities are not related by a simple linear regression and other parameters are required to obtain a predictive model. These parameters were not investigated in this work and will be objective of further studies.

The development of a method to estimate TCN could lead, in the future, to measurement campaigns focused on the study of tyre/road interaction using this approach.

3. State-of-the-art

Tyre/Road interaction yields two main noise generation mechanisms which contribute to outside emission (Sandberg and Ejsmont, 2002; Li, 2018a; Li, 2019):

- *vibro-dynamic* noise produced by the tyre vibrations due to the impact of the tyre tread against the road surface, also known as structure-borne noise;
- *aerodynamic* noise, caused by the compression and subsequent expansion of the air trapped between the tyre tread and the road surface, also known as airborne noise.

On the other hand, the only source of TCN is vibro-dynamic noise produced by the tyre rubber belt, only related to road texture properties and tyre tread geometry. The sound pressure field inside the tyre cavity moreover is influenced by the tyre torus resonances, which can be modelled accurately by using an analytic approach (Mohamed et al., 2013). A series of solution have also been proposed to mitigate tyre cavity resonances, which can also produce low frequency tonal components in outside emission (Mohamed, 2017). These solutions are based on the insertion of sound absorbing materials inside the tyre cavity, such as foams (Wang et al., 2014), mineral fibres (Haverkamp, 2001) and liners inside the tyre cavity (Baro and Åbom, 2016).

In order to monitor the acoustic performance of road surfaces, different methods of measuring Tyre/Road Noise (TRN) have been developed. In particular, sound pressure due to tyre/road pavement interaction can be detected using microphones placed in various configurations with respect to the source. Typical configurations include roadside microphones or microphones placed close to the tyre. A roadside placement aims at measuring the far-field noise of a moving vehicle from the interaction between the road surface and the tyre, while microphones placed in close proximity of the tyre measure the near-field noise produced by tyre/road interaction. The former category includes different kinds of Pass-By measurement procedures, such as the Statistical Pass-By (SPB) (ISO 11819-1:1997, 2017), Controlled Pass-By (CPB) (NF S31-119-2, 2000) and Coast-By (CB) (ISO 13325:2019,), while the latter includes techniques like the On-Board Sound Pressure (OBSP) and the CPX method.

Several studies focused on the relationship between CPX data and roadside levels measured with the CPB or SPB methods (Licitra et al., 2016; Cesbron and Klein, 2017). In particular, Licitra et al. (2016) compared the difference between CB and CPX levels on several road low-noise surfaces, finding that a simple difference between the two noise levels that could act as a propagation filter was not possible. However, despite this evidence, the difference between CPB and CPX data lied within 21 dB(A) - 24 dB(A), depending on the type of pavement and the speed of the vehicle. Indeed, when measurements performed on the same surface were compared, the correlation between CPX and CPB resulted remarkably high. This result was confirmed by Cesbron and Klein (2017), who modelled the difference ΔL between broadband CPX and CB levels using a linear relation derived from statistical analysis of the results on different road pavements:

$$\Delta L = L_{CPX} - L_{CB} \tag{1}$$

The value of $\Delta L = 21.6 \pm 0.9$ dB(A) was obtained through linear regression of experimental data and is close to the values reported by Licitra et al. (2016).

Another possibility, opposed to the previous techniques, is to measure noise inside the tyre cavity during normal vehicle motion, by using a microphone fitted to the wheel rim inside the tyre, also known as Tyre Cavity Microphone (TCM). The first example of TCM was developed at the University of Stuttgart, Germany in 1981 by Bschorr (Bschorr et al., 1981), while the method used in this paper uses the equipment developed at Karlsruhe Institute of Technology by Masino et al. (2016) on the basis of Krauss and Gauterin (2012). Tyre Cavity Noise (TCN) measurements provide an effective way of predicting several road surface characteristics, such as the grain distribution (Masino et al., 2017b), and also provide a way to detect a pavement's wear status (Masino et al., 2017a); however, up to now the main focus of TCN studies were related to optimising vehicle interior noise (Pinay et al., 2018; Sakata et al., 1990) for passenger's comfort. The identification of the wear status of pavements is also an extremely important topic, as shown by Ramos-Romero et al. (2019). Indeed, they showed the possibility of identifying four different classes of pavement wear from noise measurements from a single microphone installed at rear-right tyre proximity, as also suggested by other studies (Alonso et al., 2015). Another possibility to study the acoustic status of a road surface is to use low-cost sensors, such as smartphones (Abbondati et al., 2021) or purposely designed sensor boxes (Van Hauwermeiren et al., 2021). Despite low-cost sensors can be deployed in great numbers at once, their data is however opportunistic, and therefore requires particular calibration processes. Nevertheless, some studies have been performed to correlate TCN to exterior noise, since, for example in 2012 Krauss (Krauss and Gauterin, 2012) showed that both CPX levels and TCN were affected by road surface characteristics, providing no information however on their mutual relation. Indeed, this relation is somewhat complex to find, since noise measured in reverberant field inside the tyre is greatly affected by the tyre geometry, which distorts the spectral shape of noise (Li, 2018b). Despite these differences, Pinay et al. (2018) showed the possibility of predicting broadband CPX noise from TCN measurements, using a procedure based on linear regression. They found that the SPL measured with the CPX method was poorly predicted by the SPL inside the tyre cavity alone, but a higher prediction quality was obtained by introducing variables related to the pavement surface, such as the MPD, and other parameters related to the tyre, namely its inflation pressure and internal temperature. Interaction and quadratic terms were also added to enhance the accuracy of the model.

Del Pizzo et al. (2020) has shown that CPX noise is well correlated with road surface properties, such as spectral indicators like macro and megatexture levels defined in the ISO 13473-4 (ISO 13473-4:2008 2008). Synthetic indicators such as the MPD (ISO 13473-1:2019 2019) also well correlate with noise emission (Sandberg and Ejsmont, 2002). Therefore, in order to reduce the impact of TRN, several solutions concerning low-noise pavements have been proposed. Low-noise pavements offer a good noise reduction and represent an optimal solution, since they act directly on the sound power of the source and do not require modifications in city planning.

Among the several low-noise solutions, one of the most widespread on the Italian territory is the use of rubberized surfaces, which incorporate retreated rubber inside their mix. Depending on the phase in which the rubber is added to the mix, these surfaces are divided in *dry* and *wet*. In the dry process, crumb rubber is added to the aggregates before adding the binder, as a substitute for a part of mineral aggregate in the mixture. In these pavements, noise reduction is linked to lower macrotexture levels compared to DAC. Clogging and changes of surface texture affect the durability of these surfaces, and a model capable of predicting the acoustic ageing of rubberized road surfaces was developed (Licitra et al., 2019). However, crumb rubber addition could lead to an increase in noise levels caused by stick-and-snap enhancing (Ongel and Harvey, 2010). In the wet process, crumb rubber is thoroughly mixed with the bitumen, where it rests for 45 to 60 min (Presti, 2013). This process is also known as asphalt rubber and is defined as (ASTM International, 2008):

> a blend of asphalt binder, reclaimed tyre rubber and additives in which the rubber component is at least 15% by weight of the total blend and has reacted in the hot asphalt binder sufficiently to cause the swelling to the rubber particles.

In general, the acoustic performance of these pavements shows mixed results (Mikhailenko et al., 2020); however, mechanical and fatigue performance resulted improved compared to DAC (Kim et al., 2014). Moreover, a series of results indicate that rubberized pavements show a greater noise reduction induced by higher short-wavelength texture compared to traditional DAC surfaces, probably caused by less air compression within the air voids formed at the tyre/road interface (de León et al., 2020). Moreover, Licitra et al. (2015b) found that rubberized road surfaces seem 'a very efficient mitigation technology, providing the installation have been carried out with care and proficiency'. These results were derived from measurements performed within Leopoldo project framework (Licitra et al., 2015a).

It has also been shown that pavements which possess deep grooves are less aggressive from an acoustic point of view, compared to road surfaces that present pronounced peaks (Vieira et al., 2019). In this light, the concept of *tyre envelopment* of a road surface becomes relevant, since it aims to calculate the part of a road surface actually in contact with the tyre. The result, often called *enveloped profile*,

can be obtained through solving the integral equation of the boundary of the tyre/road interface (Klein and Hamet, 2004) or by using approaches derived from experimental measures, such as the one developed by Goubert and Sandberg (2018). This latter procedure was used to derive enveloped texture levels, which correlate better to CPX levels compared to texture levels obtained from raw road profiles (Del Pizzo et al., 2020).

4. Experimental methods

CPX, TCN and road profile measurements were performed using the same protocol for each site. All the equipment needed for the measurements was mounted on a Mercedes-Benz Vito, used as a *mobile laboratory*. This vehicle offers the right compromise in engine performance and internal space availability, while also being able to mount the CPX reference tyre SRTT, where the microphone for TCN measurements was also placed. The 24 road surfaces analysed are placed all across the Italian territory and are part of a long-term monitoring campaign performed by IPOOL srl, an Italian spin-off company of the CNR. The main characteristics of the pavements are reported in Table 1. The data-set is composed of 20 low-noise surfaces: 14 dry rubberized surfaces, 4 wet rubberized surfaces and 2 optimized texture, plus 4 DAC surfaces used as a reference.

For each site, the MPD and the texture spectral indicators in one-third-octave-bands were calculated. The road profile was also processed through an algorithm capable of simulating the tyre deformation due to the contact with the road surface, developed by Goubert and Sandberg (2018). The resulting *tyre envelopment* was then used to obtain the actual texture in contact with the tyre and spectral indicators were recalculated using this procedure. CPX and TCN measurements were also carried out simultaneously, following the procedures described in Sections 4.2 and 4.3. The correlation coefficient between TCN and texture properties was then calculated and the results were used to provide a model capable of forecasting TCN at frequencies lower than 1 kHz from texture measurements. A qualitative study of the relationship between TCN levels and outside emission was also brought about, showing that low-frequency noise inside the tyre cavity is well correlated to CPX levels.

4.1. Road texture measurements

Road texture measurements were performed with a self-developed profilometer compliant to ISO 13473 standards for macro and megatexture measurements. The hardware used is composed by:

- a laser triangulation sensor Microtrak 4 DTS-300-200 with spot size equal to 0.1 mm and sampling frequency 20 kHz fixed to the rear of the mobile laboratory;

Table 1
Main characteristics of the sites monitored during the measurement campaign. **MAS**: Maximum Aggregate Size, **MPD**: Mean Profile Depth, **DAC**: Dense Asphalt Concrete.

Site	Pavement Type	Recycling method	MAS [mm]	MPD [mm]	Age [months]
1	Gap Graded	Dry	8	0.30 ± 0.09	49
2	Gap Graded	Dry	8	0.31 ± 0.09	49
3	DAC	None	12	0.29 ± 0.05	49
4	DAC	None	12	0.30 ± 0.05	49
5	Gap Graded	Dry	8	0.44 ± 0.10	49
6	Gap Graded	Dry	8	0.62 ± 0.1	49
7	Gap Graded	Dry	16	0.73 ± 0.1	57
8	Gap Graded	Dry	16	0.72 ± 0.1	57
9	Gap Graded	Dry	16	1.13 ± 0.09	57
10	Gap Graded	Dry	16	1.23 ± 0.1	57
11	Gap Graded	Dry	12	1.07 ± 0.11	39
12	Gap Graded	Dry	12	0.90 ± 0.1	39
13	Gap Graded	Dry	12	0.59 ± 0.09	20
14	Gap Graded	Dry	12	0.52 ± 0.09	20
15	Opt. text	Wet	8	0.26 ± 0.05	17
16	Opt. text	Wet	8	0.24 ± 0.05	17
17	Dense Graded	Dry	12	0.64 ± 0.05	17
18	Dense Graded	Wet	12	0.54 ± 0.08	17
19	Optimized Texture	None	12	0.59 ± 0.06	17
20	DAC	None	12	0.52 ± 0.04	17
21	DAC	None	12	0.45 ± 0.06	17
22	Optimized Texture	None	12	0.52 ± 0.07	17
23	Dense Graded	Wet	12	0.60 ± 0.09	17
24	Dense Graded	Dry	12	0.71 ± 0.08	17

- a piezoelectric accelerometer B&K 4507B capable of measuring the vertical displacement of the road surface;
- a rotary encoder ELTRA EL63D10S5 that measures the angular displacement of the left rear tyre of the mobile laboratory, with 10 square pulses per revolution.

The signal from the laser triangulation sensor was captured through a LabVIEW code used to save data in little-endian binary double-precision floating-point format. Invalid readings that can occur during the measurement were replaced by values obtained through linear interpolation of the profile. Their percentage over the total number of data samples was monitored in order to comply to ISO 13473-1 guidelines (ISO 13473-1:2019,). The accelerometer and the encoder were connected to an Apollo light acquisition module version Apollo_lt_8C, which saved the signals in individual WAV files with 24 bits per sample and a sampling frequency of 51.2 kHz. The road profile was measured once in each direction. The accelerometer signal provided an inertial reference for subtracting the vertical oscillations of the vehicle, while the signal from the rotary encoder was used to resample the time-domain laser displacement signal to a constant step equal to 0.5 mm.

From the road profile, one-third-octave band texture levels and MPD values were calculated following the guidelines in (ISO 13473-4:2008,; ISO 13473-1:2019,). For this purpose, the road profile was divided in segments long 20.20 m. Each segment was further subdivided in 10 sub-segments and the texture levels for each segment were obtained by using the median value within the sub-segments. The uncertainty of the texture levels over a section was computed by taking into account both data variability and the uncertainty due to the use of a finite signal to estimate the texture level, according to the following equation:

$$\Delta L_{tx,i}(k) = \sqrt{\mathrm{Var}\left(L_{tx,j}(k)\right) + \delta^2_{meas}(k)} \tag{2}$$

where:

- $\Delta L_{tx,i}(\lambda)$ is the uncertainty of the segment texture level within the band centred at the spatial frequency k, defined as the inverse of the wavelength λ;
- $\mathrm{Var}\left(L_{tx,j}(k)\right)$ is the sample variance of the 10 texture level values for each wavelength within a segment;
- $\delta^2_{meas}(k)$ is the measurement uncertainty, estimated assuming a white Gaussian noise within the one-third-octave-band.

The measurement uncertainty for each section is a function of the bandwidth $\Delta k = k\left(10^{\frac{1}{20}} - 10^{-\frac{1}{20}}\right)$ and the segment length L_{seg}:

$$\delta_{meas}(k) = 5\log\left(1 + \frac{1}{\sqrt{\Delta k L_{seg}}}\right) - \log\left(1 - \sqrt{\Delta k L_{seg}}\right)^{-1} \tag{3}$$

The inverse square of the uncertainties defined for each section by Eq. 2 were then used to calculate the weighed average of the texture level of the pavement within each one-third-octave band, thus reducing the influence of sections which present great data variability from the computation of the average value:

$$\begin{cases} w_i\left(k\right) = \dfrac{1}{\Delta L^2_{tx,i}\left(k\right)} \\ \\ \overline{L}_{tx}\left(k\right) = \dfrac{\sum w_i\left(k\right) L_{tx,i}\left(k\right)}{\sum w_i\left(k\right)} \end{cases} \tag{4}$$

The uncertainties on the average one-third-octave-band levels provided by Eq. 4 are equal to:

$$\Delta\overline{L}_{tx}\left(k\right) = \sqrt{\mathrm{Var}\left(L_{tx,i}\left(k\right)\right) + \frac{1}{\sum w_i}} \tag{5}$$

MPD values are computed on baselines long 100 mm. After the calculations performed according to ISO 13473-1 (ISO 13473-1:2019,), the calculation of the average MPD value is performed assuming a log-normal distribution of the MPD, since, by definition MPD values cannot be negative. To this end, for each segment the mean ($M_{seg,i}$) and the standard deviation ($\sigma_{seg,i}$) of the natural logarithm of MPD values were calculated. Then, scatter intervals for MPD values $\left[MPD^-_{seg,i}, MPD^+_{seg,i}\right]$ were derived:

$$\begin{cases} MPD^+_{seg,i} = e^{M_{seg,i}+\sigma_{seg,i}} \\ MPD^-_{seg,i} = e^{M_{seg,i}-\sigma_{seg,i}} \end{cases} \tag{6}$$

The median value of the log-normal distribution, equal to $e^{M_{seg,i}}$ was also chosen as the MPD value within a segment $MPD_{seg,i}$.

The MPD value of the installation was calculated from the weighed average of the $MPD_{seg,i}$ across all the installation by using the

same approach of Eq. 4.

$$\begin{cases} w_i = \left(MPD^{+}_{seg,i} - MPD^{-}_{seg,i}\right)^{-2} \\ \overline{MPD} = \dfrac{\sum w_i MPD_{seg,i}}{\sum w_i} \end{cases} \tag{7}$$

The uncertainty related to the weighed mean MPD value was calculated by summing two contributions, one related to spatial variability and the second one due to the propagation of uncertainty on weighed mean values:

$$\Delta\overline{MPD} = \sqrt{\mathrm{Var}\left(MPD_{seg,i}\right) + \frac{1}{\sum w_i}} \tag{8}$$

The main advantage in using the log-normal distribution for calculating the MPD as opposed to using mean and standard deviation within a segment is that the confidence intervals obtained for the MPD values remain strictly positive for each interval, thus maintaining a physical interpretation even when data variability is high within a segment. Indeed, when pavement defects, such as joints, potholes and cracks are present, the standard deviation of the MPD can become larger than the MPD itself, thus leading to an incorrect estimation of the confidence interval of the MPD. Moreover, the log-normal distribution rapidly converges to a normal distribution for high values of the mean compared to the standard deviation and, therefore, results obtained on pavements with little inhomogeneities do not differ with standard calculations compliant with the ISO 13473-1 (ISO 13473-1:2019,).

In order to simulate the part of the road surface in direct contact with the tyre, a tyre envelopment algorithm was used. This algorithm was developed from experimental measurements performed on the SRTT, as shown by Goubert and Sandberg (2018). Del Pizzo et al. (2020) have also shown that the texture levels calculated from the tyre envelopment correlated better with CPX noise levels compared to texture levels calculated directly from the raw profile. Indeed, tyre envelopment can provide an effective way of distinguishing positive and negative texture, which act differently on the acoustic performance of road pavements.

The results of texture measurements on the road surfaces are presented in Section 5.1.

4.2. CPX measurements

CPX measurements were performed according to the last ISO 11819-2 release using protocol derived from Licitra et al. (2014). The measuring equipment is composed by:

- two class-1 GRAS 40AE 1/2" prepolarized free-field microphones placed close to the rear right tyre of the mobile laboratory, as suggested by ISO 11819-2:2017 (ISO 11819-2:2017,);
- the same rotary encoder used for road profile measurements.

The signals were acquired using an Apollo light version Apollo_lt_8C and stored in WAV format with 24 bits per sample sampled at 51.2 kHz.

Since it is known that TRN is greatly influenced by the vehicle's speed, in order to perform comparisons between the acoustic performance of different pavements, it is necessary to calculate the CPX level at a reference speed. This was achieved for each site through the measurement of the sound pressure produced at different runs on the road surface, at different speeds. During the post processing phase, the road surface was divided in segments 20.20 m long. Within each segment, the signal from each microphone was filtered using a class-1 one-third-octave-band filter bank. Under the assumption of white Gaussian noise within each band, for each microphone the RMS values and the variance of the RMS signal for each segment was calculated. Then, the average RMS value between the two microphones was calculated with its uncertainty ($\overline{p}^2_{seg}, \Delta\overline{p}^2_{seg}$) and the SPL were derived:

$$L_{CPX,seg} = 10\log\frac{\overline{p}^2_{seg}}{p^2_0} \tag{9}$$

The uncertainty on the $L_{CPX,seg}$ was also estimated calculating the maximum variation of the RMS values:

$$\begin{cases} \Delta L^{+}_{CPX,seg} = 10\log\left(1 + \dfrac{\Delta\overline{p}^2_{seg}}{\overline{p}^2_{seg}}\right) \\ \Delta L^{-}_{CPX,seg} = 10\log\left(1 - \dfrac{\Delta\overline{p}^2_{seg}}{\overline{p}^2_{seg}}\right)^{-1} \end{cases} \tag{10}$$

This data was used to perform a linear regression between the one-third-octave-band SPL and the logarithm of the vehicle speed, according to the equation:

$$L_{CPX,seg}\left(f_{ci}\right) = A_{CPX}\left(f_{ci}\right)\log\frac{v_{seg}}{v_0} + B_{CPX}\left(f_{ci}\right) \tag{11}$$

where:

- f_{ci} is the central frequency of the i^{th} one-third-octave band;
- $L_{CPX,seg}(f_{ci})$ is the sound pressure level averaged between the two microphones within the band centred at f_{ci};
- v_{seg} is the vehicle speed within the segment and v_0 is the reference speed, set to $50\,\frac{\text{km}}{\text{h}}$.;
- $A_{CPX}(f_{ci})$ and $B_{CPX}(f_{ci})$ are the regression coefficients for each band.

In order to take into account the asymmetry of the uncertainties on one-third-octave SPL values, the *multifit* procedure (Licitra et al., 2014), based on an iterative minimum χ^2 algorithm, was used. From the regression coefficients, it is possible to calculate the one-third-octave-band CPX levels for each segment at the speed of $50\,\frac{\text{km}}{\text{h}}$ ($\overline{L}_{CPX,seg}$) with 68% confidence intervals ($\Delta\overline{L}_{CPX,seg}$) for each segment, thus providing an estimate of the standard deviation of the $L_{CPX}(f_{ci})$ values. Moreover, the last ISO release provides corrections for temperature (ISO/TS 13471-1:2017,), hardness (ISO 11819-3:2017,) and vehicle influence (ISO 11819-2:2017,) on measurements, through the linear relation:

$$L_{CPX,seg,Corr}\left(f_{ci}\right) = L_{CPX,seg} - \gamma\left(T - T_0\right) - \beta\left(H - H_0\right) + C\left(f_{ci}\right) \tag{12}$$

where:

- $L_{CPX,seg,Corr}(f_{ci})$ is the corrected CPX level in one-third-octave bands;
- γ and β are the temperature and hardness coefficients;
- $T_0 = 20\ ^{\circ}\text{C}, H_0 = 66$ Shore(A) are the temperature and hardness reference values;
- $C(f_{ci})$ is the correction for reflections from the vehicle, measured according to ISO/TS 11819-3 (ISO 11819-3:2017,).

Despite temperature and hardness coefficients reported in the ISO standards are strictly valid only for broadband levels, they were applied to one-third-octave band levels altogether, since a detailed modelling of the frequency relationship between hardness, temperature and tyre noise emission is not yet established. Nevertheless, the use of Eq. 12 provides a straightforward way to normalise noise levels to reference conditions.

Lastly, for each surface, the weighed mean of the CPX levels was calculated on the installation, using the inverse of the square of the confidence interval. The uncertainty on the CPX level of each surface was estimated by summing the contribution of the spatial variability of the installation, obtained through the sample variance, and the propagation of the uncertainty of the weighted mean.

4.3. TCN measurements

TCN measurements were performed using a system developed at Karlsruhe Institute of Technology (KIT) by Masino et al. (2016). It is based on the following components:

- a CUI Devices cma-4544pf-w electret microphone placed inside the tyre cavity, purposely modified for measuring higher sound pressure values;
- a BC127 Bluetooth 5 module attached to the tyre rim inside a circular encasing built to provide support to the device and its power. This module also converts the microphone signal to 16 bits per sample digital output sampled at 44.1 kHz;
- a Raspberry Pi 2 model B version 1.1 placed on board of the vehicle that stores the data locally and is then connected to a laptop through Ethernet cable to download the data after measurements.

Since TCN is also influenced by the speed of the vehicle, a measurement and data post-processing procedure was designed in order to normalise the measurements to a reference speed, in a similar fashion to the CPX measurements. In particular, the method consists in performing several runs on the pavement at different speeds, each time recording the audio signal provided by the microphone and the square pulses of the encoder. During the post-processing phase, one-third-octave band levels were obtained from 100 to 5000 Hz and the average one-third-octave band levels were fitted with the decimal logarithm of the vehicle speed, according to the equation:

$$L_{p_{int}}\left(f_{ci}\right) = A\left(f_{ci}\right)\log\frac{v}{v_0} + B\left(f_{ci}\right) \tag{13}$$

where:

- f_{ci} is the central frequency of the i^{th} one-third-octave band;
- $L_{p_{int}}(f_{ci})$ is the sound pressure level inside the tyre cavity within the band centred at f_{ci};
- v is the average run speed and v_0 is the reference speed, set to $50\,\frac{\text{km}}{\text{h}}$;
- $A(f_{ci})$ and $B(f_{ci})$ are the regression coefficients for each band.

For each surface, the regressions defined by Eq. 13 is the used to calculate the SPL inside the tyre cavity in one-third-octave bands at the speed of 50 $\frac{\text{km}}{\text{h}}$ with prediction intervals at a 68% confidence level. The estimation of the SPL at the same speed on all the different surfaces is fundamental in order to compare their acoustic performance, both for outside emission and noise inside the cavity.

5. Results

5.1. Road Texture, CPX and TCN Results

One-third-octave-band levels were calculated for the 24 different surfaces. The boxplot of the raw texture levels is shown in Fig. 1. This boxplot shows that data is well distributed across all the wavelengths analysed.

The results of the envelopment process described by Goubert and Sandberg (2018) are shown in Fig. 2. Enveloped texture levels are lower than the regular texture levels defined in ISO 13473-4:2008 (2008) calculated from the raw profile. This can easily explained taking into account the interpretation of the enveloped texture as the part of the road profile actually indented into the rolling tyre and, therefore, it does not necessarily cover the whole texture depth.

The boxplot of the one-third-octave-band CPX levels from 315 to 5000 Hz on the 24 surfaces is shown in Fig. 3. Data shows a wide variability in each band, ranging from almost 10 dB at low frequency to 4 dB at 1250 Hz. Therefore the pavements used for this study are different from an acoustical point of view.

The boxplot of the one-third-octave-band TCN levels from 100 to 5000 Hz on the 24 surfaces is shown in Fig. 4. Interestingly, the great variability shown by TCN at 200 Hz is mainly due to the presence of few outliers, since the interquartile range is narrow compared to the data range. This behaviour, also present at 400 Hz, is explained by taking into account the tyre cavity resonances. As a matter of fact, the circular modes of the tyre cavity can be described by the following equation (Mohamed et al., 2013):

$$f_n = n\frac{c}{\pi}\frac{1}{R_{in}+R_{out}} \rightarrow f_1 \approx 215 \text{ Hz} \tag{14}$$

where:

- $n \in \mathbb{N}$ is the mode order;
- $c = 343 \text{ ms}^{-1}$ is the speed of sound in air at 20 °C;
- $R_{in} = 0.191$ m is the inner tyre radius;
- $R_{out} = 0.317$ m is the outer tyre radius.

Another interesting aspect, whose possible explanation is presented in Section 7, is that frequencies higher than 1600 Hz do not show great variability across the different surfaces.

From the two boxplots in Figs. 3 and 4 it is clear that outside noise emission and noise inside the tyre cavity are quite different: while CPX outside emission results in rather broad peak centred at 800 Hz, TCN presents more peaks, caused by the tyre cavity resonances and their harmonics.

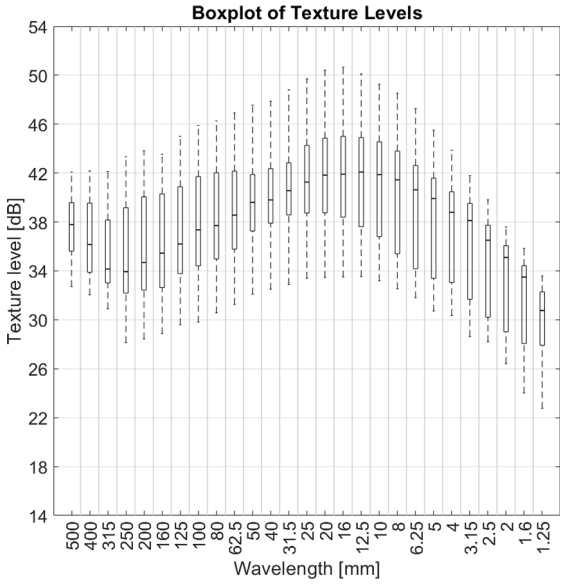

Fig. 1. Boxplot of one-third-octave-band texture levels from 500 mm to 1.25 mm. Whiskers cover maximum and minimum values, while the boxplot include the first and third quartiles. The line within the boxplots is the median value of the distribution.

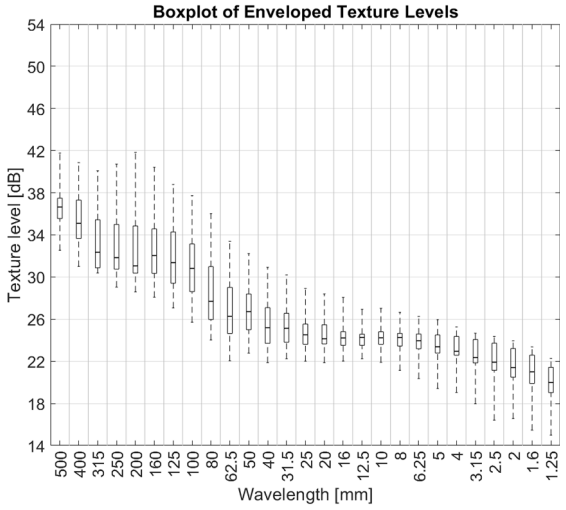

Fig. 2. Boxplot of one-third-octave-band enveloped texture levels from 500 mm to 1.25 mm. The whiskers cover maximum and minimum values, while the boxplot include the first and third quartiles. The line within the boxplots is the median value of the distribution.

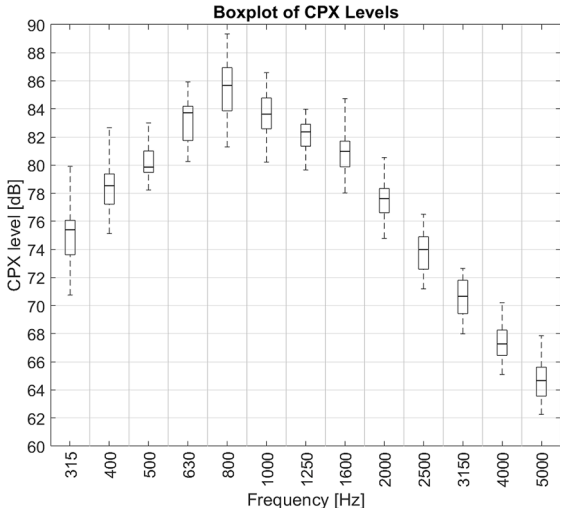

Fig. 3. Boxplot of one-third-octave-band CPX levels from 315 Hz to 5000 Hz. Whiskers cover maximum and minimum values, while the boxplot include the first and third quartiles. The line within the boxplots is the median value of the distribution.

5.2. Correlation between TCN and road surface parameters

The correlation coefficient between each couple of texture one-third-octave band and TCN one-third octave band was calculated. The results, shown in Fig. 5 for the texture levels derived from the road profile and in Fig. 6 for the correlation coefficient between TCN and tyre envelopment, show that TCN is positively correlated to road texture at almost every band. The correlation is high ($r \geqslant 0.7$) for frequencies between 160 and 1600 Hz, while it becomes negligible at higher frequencies. This is consistent with studies on outside emission that link the low frequency region to vibrations of the tyre rubber, induced by the asperities found on the road surface. The negative correlation with road texture, found in high frequency outside emission, is not present in TCN, in accordance with the hypothesis that the main source of high frequency noise is the air-pumping phenomenon. Interestingly, the correlation coefficient results more concentrated in the texture wavelengths from 10 to 315 mm using the enveloped texture, while texture levels calculated from the raw profile result correlated with TCN even at lower wavelengths.

Since the MPD represents a synthetic indicator capable of providing a rough estimate of the superficial properties of a pavement, its values on the 24 sites were also correlated with the one-third-octave-band TCN levels. The result is shown in Fig. 7. Again, very high correlation was found between the MPD and TCN from 315 to 1000 Hz, with other correlation spikes at 200 Hz and 1600 Hz.

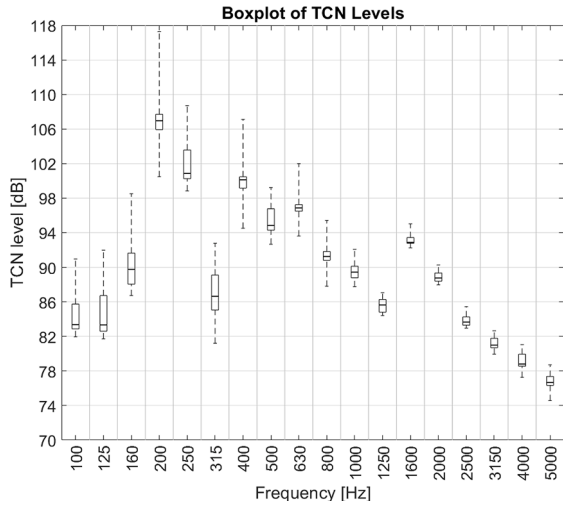

Fig. 4. Boxplot of one-third-octave-band TCN levels from 100 Hz to 5000 Hz. Whiskers cover maximum and minimum values, while the boxplot include the first and third quartiles. The line within the boxplots is the median value of the distribution.

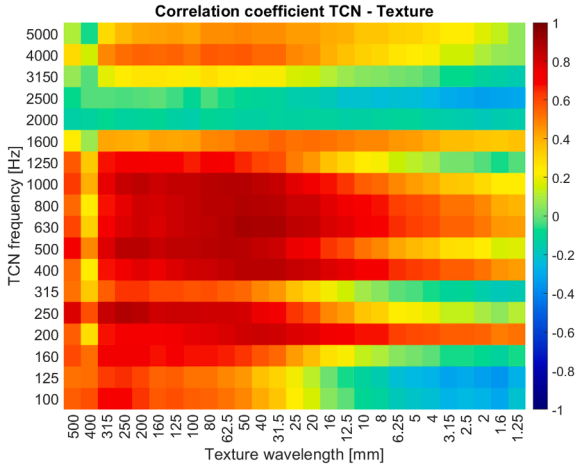

Fig. 5. Correlation heatmap between TCN and road texture.

5.3. *Correlation between TCN and CPX levels*

Noise inside the tyre cavity does not correlate well with noise emission measured through the CPX method at all frequencies, as shown in Fig. 8. Indeed, it appears that CPX frequencies lower than 1 kHz show medium to high correlation ($r \leqslant 0.7$) with almost all TCN bands, except the bands at 100, 125, 2000 and 2500 Hz. This can be explained by taking into account the different generation mechanisms that are present inside and outside the tyre: while tyre vibrations are the main source of noise at frequencies lower than 1 kHz, higher frequencies are related to air pumping and are thus non measurable inside the tyre cavity. On the other hand, noise at very low frequency ($<$ 315 Hz) was not recorded during CPX measurements since it is not required by ISO 11819-2:2017 (2017). Despite the high correlation found, noise within the low-frequency (315-1000 Hz) TCN and CPX band result not linked by a linear model, since a linear regression between the two quantities does not yield satisfactory results, as shown in Fig. 9. It seems, therefore, that even for the low frequency region, more information is needed to provide a model capable of forecasting CPX noise levels from TCN; however, TCN can be a good indicator of CPX levels, given the high correlation found at LF.

6. TCN modelling

From the results reported in Section 5.2, the one-third-octave-bands of TCN were grouped in different wide-bands shown in Table 2, using an approach derived from CPX data analysis presented by de León et al. (2020) and Del Pizzo et al. (2020). The SPL within each wide-band was calculated using the well-known formula:

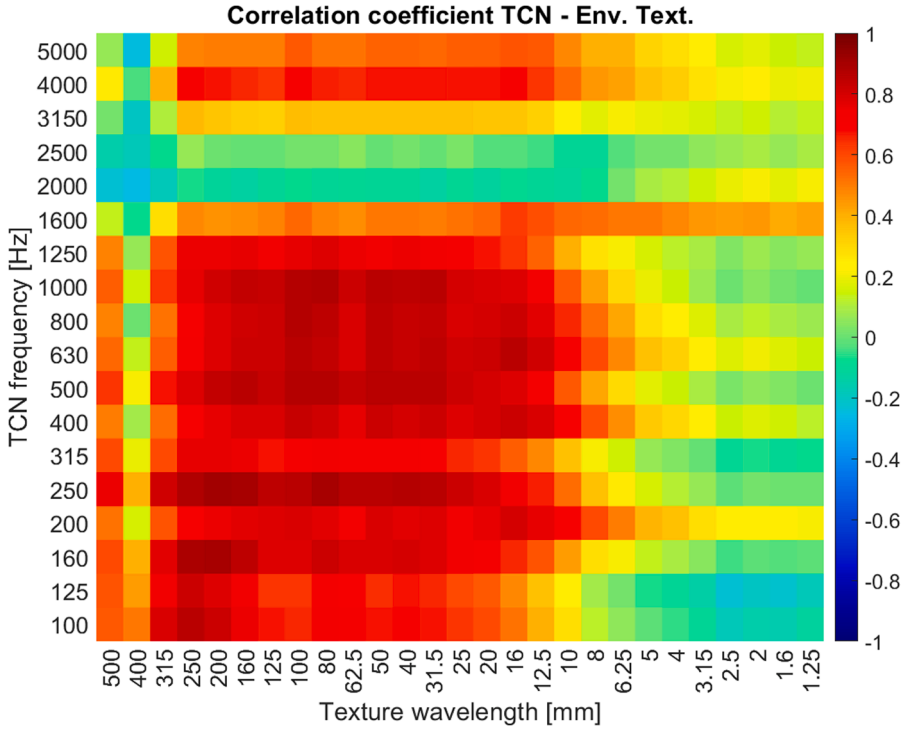

Fig. 6. Correlation heatmap between TCN and enveloped road texture.

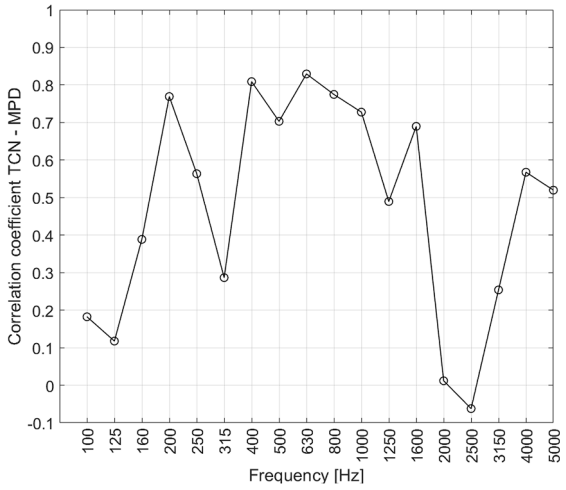

Fig. 7. Correlation coefficient between TCN and MPD.

$$L_{p_{int}}\left(wb\right) = 10\log\sum 10^{\frac{L_{p_{int}}\left(f_i\right)}{10}} \tag{15}$$

where:

- $L_{p_{int}}(wb)$ is the SPL within a wide-band;
- $L_{p_{int}}(f_i)$ is the SPL of the one-third-octave band centred at f_i.

The wide-bands derived from Eq. 15 were then correlated with the enveloped texture levels (Fig. 10).
Enveloped texture bands that showed a correlation coefficient higher than 0.7 for VLF and LF bands were then used for a Principal

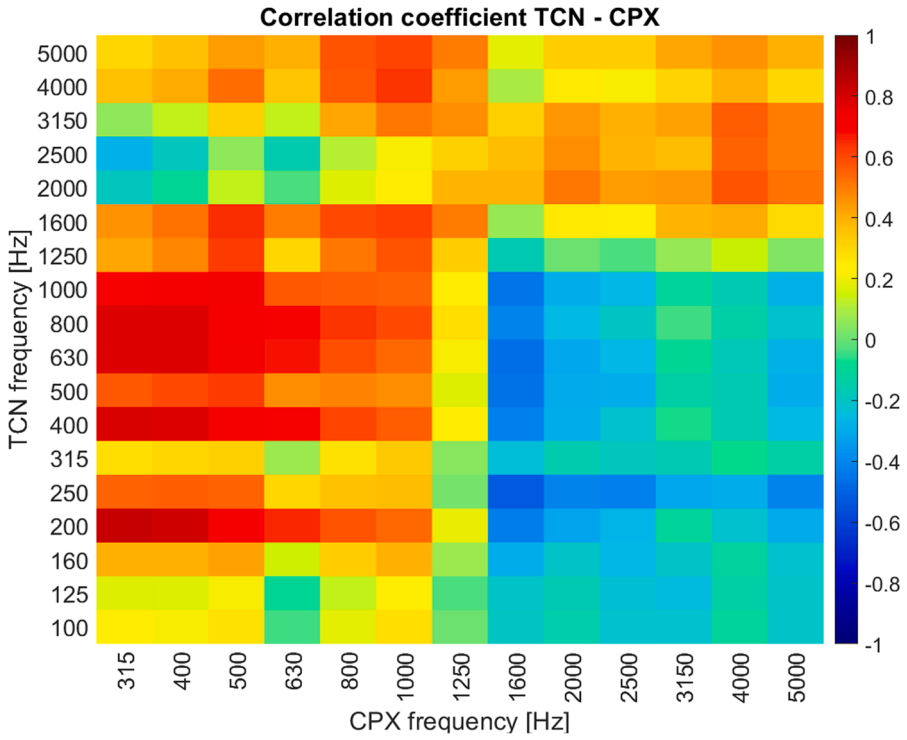

Fig. 8. Correlation heatmap between TCN and CPX values.

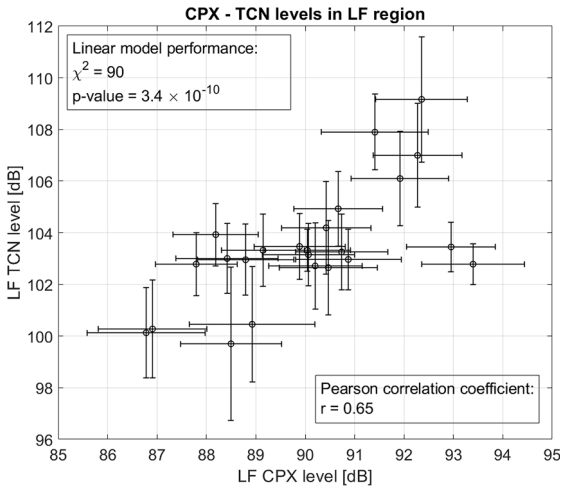

Fig. 9. LF TCN and LF CPX data and linear model performance.

Table 2
Wide-bands for TCN modelling.

Wide-band	One-third-octave-bands [Hz]
Very Low Frequency (VLF)	100–250
Low Frequency (LF)	315–1000
Mid Frequency (MF)	1250–2500
High Frequency (HF)	3150–5000

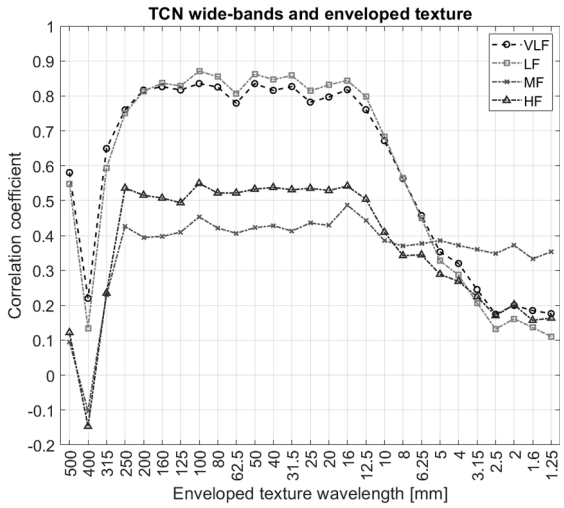

Fig. 10. Correlation coefficient between the wide-band TCN levels and the one-third-octave-band enveloped texture levels.

Component Analysis (PCA), in order to reduce the number of variables while limiting the loss of information. The first two principal components together explain 97.47% of the total variance of enveloped texture levels and, therefore, were analysed in depth. The matrix of the first two principal components is shown in Table 3. As shown in Table 3, the first principal component shares similar coefficients for all wavelengths, while the second principal component has positive coefficients from 12.5 to 25 mm and negative coefficients for the wavelengths from 31.5 to 250 mm.

Since the first principal component explains almost 94% of the total variance, and its coefficients are almost constant for each variable, it can be inferred that all texture wavelengths provide the same information. It was therefore possible to use the actual physical variables in place of the first principal component and choose the texture one-third-octave-band most correlated with TCN wide-bands to perform a linear regression to model TCN as a function of road surface properties.

The linear regression was performed between the VLF and VF TCN and the 100 mm texture band, while it was not performed on MF and HF due to the poor correlation shown with road texture. A minimum χ^2 algorithm was used to derive the model coefficients, taking into account uncertainties on both variables, since the uncertainties of the independent variable are comparable to the dependent ones.

The regression coefficients for the two models are shown in Table 4. The p-values obtained indicate the probability of observing a test statistic as extreme as, or more extreme than the observed values, assuming that the model is true. Therefore, large p-values are indicative of a high goodness-of-fit; moreover, the reduced χ^2 statistics for both regressions is very close to unity, which also points that the models developed perform well on the experimental data (see Figs. 11 and 12).

7. Discussion

Results show that VLF and LF TCN correlate well with macro and megatexture spectral indicators with wavelengths from 12.5 mm to 250 mm and MPD. This can be easily explained taking into account the type of noise source that acts inside the tyre cavity, that is to say the vibrations of the tyre belt. These vibration are favoured by the presence of high levels of megatexture, which is also linked to

Table 3
Loadings of the first two PCA components.

Band centre [mm]	First component	Second component
12.5	0.25	0.62
16	0.26	0.44
20	0.27	0.27
25	0.27	0.12
31.5	0.27	0.00
40	0.27	−0.07
50	0.27	−0.01
62.5	0.27	−0.16
80	0.27	−0.21
100	0.27	−0.05
125	0.27	−0.07
160	0.27	−0.17
200	0.26	−0.30
250	0.25	−0.37
Variance explained [%]	93.73	3.74

Table 4
Regression coefficients and goodness-of-fit using the χ^2 distribution. The p-values were obtained from the χ^2 distribution with 24-2 d.o.f.

	VLF	LF
Intercept	81.0 ± 3.5	86.1 ± 2.5
Slope	0.89 ± 0.11	0.56 ± 0.08
χ^2	22.08	23.85
p-value	0.45	0.35

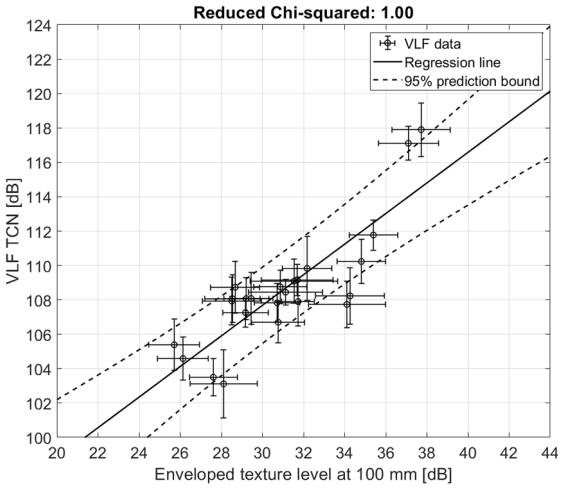

Fig. 11. Data points and linear model with 95% prediction bounds for VLF TCN.

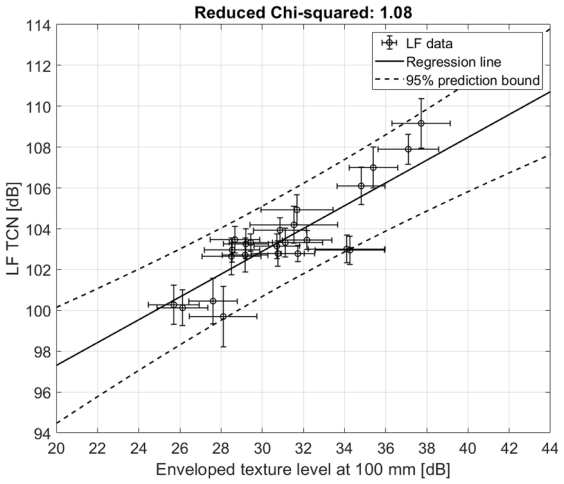

Fig. 12. Data points and linear model with 95% prediction bounds for LF TCN.

greater outside noise emission (Del Pizzo et al., 2020). Shorter wavelengths are likely unrelated to TCN, since they are linked to aerodynamic phenomena present in outside emission, like air pumping. Therefore, it could be argued that the tyre rubber acts as a filter that allows only long-wavelength components to provide the excitation required to produce noise inside the cavity. Interestingly, the analysis showed that the correlation is almost constant in this range for VLF and LF TCN and, moreover, the subsequent PCA analysis also pointed out that the texture levels within these wavelengths all provide the same information under a statistical point of view. In this light, the most correlated texture wavelength was chosen to model VLF and LF TCN in function of texture with satisfactory results, as shown by the goodness-of-fit parameters reported in Table 4.

As far as the relationship between CPX and TCN is concerned, the two noise fields result not correlated at frequencies higher than 1 kHz. This could be explained by taking into account that noise inside the tyre cavity is not affected by aerodynamic phenomena such

as the air-pumping process. In fact, air-pumping is reduced by the presence of short wavelength macrotexture, which allows the air to escape from the tyre/road interface and is an important factor for reducing outside emission. This difference, together with the distortion of the spectral shape caused by the cavity resonant frequencies, results in poor spectral correlation between TCN and CPX data.

Another possible reason is that in CPX, the sound is in free field, whereas in TCN, the sound is in reverberant field (Li, 2018b). Indeed, noise inside the tyre cavity shows moderate correlation with CPX noise levels at low frequencies ($r \gtrapprox 0.7$ for frequencies lower than 1 kHz). The low goodness-of-fit obtained for the regression between low frequency TCN and low frequency CPX levels shows that the relationship between CPX and TCN is more complex and could depend on other parameters, such as the acoustic absorption or the layer thickness. The acoustic absorption could be monitored on-site by using a contactless p-u probe capable of acquiring data simultaneously to the other instrumentation (Bianco et al., 2020), while other parameters could be derived through coring tests or the pavement job-mix formula which were not available at this stage.

8. Conclusions

In this work, Close-Proximity (CPX) noise emission, Tyre Cavity Noise (TCN) and road profile properties were correlated and analysed using an experimental approach based on measurements performed on 24 road surfaces present on the Italian territory.

Results indicate that TCN is highly correlated to megatexture properties and, moreover, it is possible to model low frequency TCN as a function of the texture level within the one-third-octave band centred at 100 mm. This points out that it is possible to monitor superficial properties of the road surface through the use of Tyre Cavity Microphones (TCMs), which have the advantage of being rugged devices, placed inside the tyre cavity and thus their measure is isolated from external noise sources.

The correlation coefficient between TCN and CPX one-third-octave-band levels also results moderately correlated, since the highest correlation coefficient between the two levels is around 0.7 at low frequencies. However, higher frequencies result uncorrelated: this is reasonably due to the different outside noise sources at the two frequency regions, differently related to road texture. A linear model results inadequate for describing the relation between low frequency TCN and low frequency CPX noise, since the χ^2 goodness-of-fit returns a p-value far from indicating a good model performance. Possibly, the influence of other parameters related to road characteristics also be investigated in the relationship between outside noise and TCN. Moreover, in this phase, the lowest CPX one-third-octave band was 315 Hz, as requested by ISO 11819-2, while TCN was monitored down to 100 Hz due to the presence of tyre cavity modes. This lower frequency bound could be impossible to remove even in future studies, since lower frequencies in CPX emission are more influenced by air turbulence rather that tyre/road noise.

Other future steps could include widening the study on different kind of porous asphalts, in order to obtain information on these pavements too and to achieve a wider applicability of the method. Another future objective could be represented by the possibility to use Artificial Neural Networks to develop a classification model capable of distinguishing the wear status of a pavement from TCN measurements, as already done with noise outside the vehicle (Ramos-Romero et al., 2019).

In order to obtain information on the time evolution of TCN on these surfaces, measurements on the same pavement at different times are required. This task, however, requires a time scale of several years, as pointed out by ageing models already developed for CPX noise (Licitra et al., 2019). Despite the pavements already have different ages, the ageing process is related to many factors that could not be taken into account at this stage and, moreover, could depend on the specific pavement, thus not making a cross-sectional analysis of the relationship between pavement age and TCN relevant at this stage.

An application currently under development is related to the detection local pavement defects such as potholes or cracks, rather than the determination of the mean values across the whole installation: while it is true that the spatial variability of TCN data, determined through the standard deviation, provides an estimation of the pavement homogeneity that should degrade over time, being able to pinpoint and identify single defects on the pavement by analysing the TCN signal could represent an additional value of this methodology.

Lastly, it could be useful to evaluate the relation of TCN with roadside far-field noise measured with Pass-By methods. This task was not performed during these measurement campaigns, since the main focus was monitoring noise using on-board equipment, but it could become an objective of future works, since it would provide a description that ranges from far-field roadside noise levels, to near-field noise measured in close proximity of the tyre and, finally, zooms into the tyre cavity.

To sum up, while TCN measurements are not yet standardised, they represent an interesting procedure to evaluate the quality of road surfaces from an acoustical point of view. TCN is indeed well correlated to road surface properties, with the advantages that its measurement can be easily performed in normal traffic flow and does not require particular attention to trailers and/or other devices protruding from the vehicle, unlike CPX and texture measures.

Acknowledgments

The authors wish to thank Daniele Fornai for sharing information and data on the pavements present in this paper.

References

Abbondati, F., Biancardo, S.A., Veropalumbo, R., Dell'Acqua, G., 2021. Surface monitoring of road pavements using mobile crowdsensing technology. Measurement 171, 108763.

Alonso, J., López, J.M., Pavón, I., Asensio, C., De Arcas, G., 2015. Road state estimation based on acoustic analysis. Securitas Vialis 7, 13–19.

ASTM International, 2008. International annual book of standards. d 8 definitions, vol. 04.03.
Babisch, W., Swart, W., Houthuijs, D., Selander, J., Bluhm, G., Pershagen, G., Dimakopoulou, K., Haralabidis, A.S., Katsouyanni, K., Davou, E., et al., 2012. Exposure modifiers of the relationships of transportation noise with high blood pressure and noise annoyance. J. Acoust. Soc. Am. 132, 3788–3808.
Baro, S., Åbom, M., 2016. Tyre cavity noise: porous materials as a countermeasure, INTER-NOISE and NOISE-CON Congress and Conference Proceedings, Institute of Noise. Control Eng.. 6730–6735.
Bianco, F., Fredianelli, L., Lo Castro, F., Gagliardi, P., Fidecaro, F., Licitra, G., 2020. Stabilization of a pu sensor mounted on a vehicle for measuring the acoustic impedance of road surfaces. Sensors 20, 1239.
Bluhm, G.L., Berglind, N., Nordling, E., Rosenlund, M., 2007. Road traffic noise and hypertension. Occup. Environ. Med. 64, 122–126.
Botteldooren, D., Dekoninck, L., Gillis, D., 2011. The influence of traffic noise on appreciation of the living quality of a neighborhood. Int. J. Environ. Res. Public Health 8, 777–798.
Bschorr, O., Mittmann, J., Wolf, A., 1981. Theoretische und experimentelle Untersuchungen zur Abstrahlung von Reifenlärm: Interim Report; Contract 522–7291-TV-79-713. Messerschmitt-Bölkow-Blohm GmbH, Ottobrunn, Germany.
Cesbron, J., Klein, P., 2017. Correlation between tyre/road noise levels measured by the coast-by and the close-proximity methods. Appl. Acoust. 126, 36–46.
Commission of the European Communities, 2008. Communication from the commission to the european parliament, the council, the european economic and social committee and the commitee of the regions - public procurement for a better environment {SEC(2008) 2124}{SEC(2008) 2125}{SEC(2008) 2126} com(2008) 400 final.
Del Pizzo, A., Teti, L., Moro, A., Bianco, F., Fredianelli, L., Licitra, G., 2020. Influence of texture on tyre road noise spectra in rubberized pavements. Appl. Acoust. 159, 107080.
Garbarino, E., Quintero, R., Donatello, S., Wolf, O., 2016. Revision of Green Public Procurement Criteria for Road Design, Construction and Maintenance. Technical report and criteria proposal. Technical Report. Joint Research Centre. Brussels, Belgium.
Goubert, L., Sandberg, U., 2018. Enveloping texture profiles for better modelling of the rolling resistance and acoustic qualities of road pavements. In: Proceedings of the 8th Symposium on Pavement Surface Characteristics, ARRB, Brisbane, Queensland, Australia, pp. 1–12.
Haverkamp, M., 2001. Solving vehicle noise problems by analysis of the transmitted sound energy. In: Proceedings of the International Seminar on Modal Analysis, KU Leuven, Leuven, Belgium. pp. 1339–1346.
ISO 11819-1:1997, 2017. Acoustics – Measurement of the influence of road surfaces on traffic noise – Part 1: Statistical pass-by method. Standard. International Organization for Standardization. Geneva, Switzerland.
ISO 11819-2:2017, 2017. Acoustics – Measurement of the influence of road surfaces on traffic noise – Part 2: The close-proximity method. Standard. International Organization for Standardization. Geneva, Switzerland.
ISO 11819-3:2017, 2017. ISO/TS 11819-3:2017 - Acoustics — Measurement of the influence of road surfaces on traffic noise —- Part 3: Reference tyres. Standard. International Organization for Standardization. Geneva, Switzerland.
ISO 13325:2019, 2019. Tyres – Coast-by methods for measurement of tyre-to-road sound emission. Standard. International Organization for Standardization. Geneva, Switzerland.
ISO 13473-1:2019, 2019. Characterization of pavement texture by use of surface profiles – Part 1: Determination of mean profile depth. Standard. International Organization for Standardization. Geneva, Switzerland.
ISO 13473-4:2008, 2008. ISO 13473-4:2008 - Characterization of pavement texture by use of surface profiles – Part 4: Spectral analysis of surface profiles. Standard. International Organization for Standardization. Geneva, Switzerland.
ISO/TS 13471-1:2017, 2017. Acoustics — Temperature influence on tyre/road noise measurement — Part 1: Correction for temperature when testing with the CPX method. Standard. International Organization for Standardization. Geneva, Switzerland.
Kim, S., Lee, S.J., Yun, Y.B., Kim, K.W., 2014. The use of CRM-modified asphalt mixtures in Korea: Evaluation of high and ambient temperature performance. Constr. Build. Mater. 67, 244–248.
Klein, P., Hamet, J.F., 2004. Road texture and rolling noise: An envelopment procedure for tire-road contact. Technical Report. hal-00546120.
Krauss, O., Gauterin, F., 2012. Analysis of tire road noise using a tire cavity sound measurement system. In: EURONOISE 2012 Conference Proceedings.
de León, G., Del Pizzo, A., Teti, L., Moro, A., Bianco, F., Fredianelli, L., Licitra, G., 2020. Evaluation of tyre/road noise and texture interaction on rubberized and conventional pavements using cpx and profiling measurements. Road Mater. Pavement Des. 1–12.
Li, T., 2018a. Literature review of tire-pavement interaction noise and reduction approaches. J. Vibroeng. 20, 2424–2452.
Li, T., 2018b. A state-of-the-art review of measurement techniques on tire–pavement interaction noise. Measurement 128, 325–351.
Li, T., 2019. A review on physical mechanisms of tire-pavement interaction noise. SAE Int. J. Vehicle Dyn., Stability, NVH 3, 87–112.
Licitra, G., Cerchiai, M., Teti, L., Ascari, E., Bianco, F., Chetoni, M., 2015a. Performance assessment of low-noise road surfaces in the leopoldo project: Comparison and validation of different measurement methods. Coatings 5, 3–25.
Licitra, G., Cerchiai, M., Teti, L., Ascari, E., Fredianelli, L., 2015b. Durability and variability of the acoustical performance of rubberized road surfaces. Appl. Acoust. 94, 20–28.
Licitra, G., Moro, A., Teti, L., Del Pizzo, A., Bianco, F., 2019. Modelling of acoustic ageing of rubberized pavements. Appl. Acoust. 146, 237–245.
Licitra, G., Teti, L., Bianco, F., Chetoni, M., Ascari, E., 2016. Relationship between pass by results, cpx ones and roadside long-term measures: some considerations. In: INTER-NOISE and NOISE-CON Congress and Conference Proceedings, Institute of Noise Control Engineering. pp. 2508–2516.
Licitra, G., Teti, L., Cerchiai, M., 2014. A modified close proximity method to evaluate the time trends of road pavements acoustical performances. Appl. Acoust. 76, 169–179.
Masino, J., Daubner, B., Frey, M., Gauterin, F., 2016. Development of a tire cavity sound measurement system for the application of field operational tests. In: 2016 Annual IEEE Systems Conference (SysCon) Proceedings. IEEE, Orlando, Florida, USA, pp. 1–5.
Masino, J., Foitzik, M.J., Frey, M., Gauterin, F., 2017a. Pavement type and wear condition classification from tire cavity acoustic measurements with artificial neural networks. J. Acoust. Soc. Am. 141, 4220–4229.
Masino, J., Pinay, J., Reischl, M., Gauterin, F., 2017b. Road surface prediction from acoustical measurements in the tire cavity using support vector machine. Appl. Acoust. 125, 41–48.
Mikhailenko, P., Piao, Z., Kakar, M.R., Bueno, M., Athari, S., Pieren, R., Heutschi, K., Poulikakos, L., 2020. Low-noise pavement technologies and evaluation techniques: a literature review. Int. J. Pavement Eng. 1–24.
Mohamed, Z., 2017. Tire cavity resonance mitigation using acoustic absorbent materials. J. Vib. Control 23, 1607–1622.
Mohamed, Z., Wang, X., Jazar, R., 2013. A survey of wheel tyre cavity resonance noise. Int. J. Veh. Noise Vib. 9, 276–293.
Muzet, A., 2007. Environmental noise, sleep and health. Sleep Med. Rev. 11, 135–142.
NF S31-119-2, 2000. Acoustique - Caractérisation in situ des qualités acoustiques des revêtements de chaussées - Mesurages acoustiques au passage - Partie 2: procédure véhicule maîtrisé. Standard. ANFOR. La Plaine Saint-Denis, France.
Ongel, A., Harvey, J., 2010. Pavement characteristics affecting the frequency content of tire/pavement noise. Noise Control Eng. J. 58, 563–571.
Ouis, D., 2001. Annoyance from road traffic noise: a review. J. Environ. Psychol. 21, 101–120.
Pinay, J., Unrau, H.J., Gauterin, F., 2018. Prediction of close-proximity tire-road noise from tire cavity noise measurements using a statistical approach. Appl. Acoust. 141, 293–300.
Presti, D.L., 2013. Recycled tyre rubber modified bitumens for road asphalt mixtures: A literature review. Constr. Build. Mater. 49, 863–881.
Ramos-Romero, C., León-Ríos, P., Al-Hadithi, B., Sigcha, L., De Arcas, G., Asensio, C., 2019. Identification and mapping of asphalt surface deterioration by tyre-pavement interaction noise measurement. Measurement 146, 718–727.
Sakata, T., Morimura, H., Ide, H., 1990. Effects of tire cavity resonance on vehicle road noise. Tire Sci. Technol. 18, 68–79.
Sandberg, U., Ejsmont, J., 2002. Tyre/road noise. Reference book. INFORMEX, Kisa, Sweden.

Selander, J., Nilsson, M.E., Bluhm, G., Rosenlund, M., Lindqvist, M., Nise, G., Pershagen, G., 2009. Long-term exposure to road traffic noise and myocardial infarction. Epidemiology 272–279.
Stansfeld, S.A., Berglund, B., Clark, C., Lopez-Barrio, I., Fischer, P., Öhrström, E., Haines, M.M., Head, J., Hygge, S., Van Kamp, I., et al., 2005. Aircraft and road traffic noise and children's cognition and health: a cross-national study. The Lancet 365, 1942–1949.
Van Hauwermeiren, W., Filipan, K., Botteldooren, D., De Coensel, B., 2021. Opportunistic monitoring of pavements for noise labeling and mitigation with machine learning. Transport. Res. Part D: Transport Environ. 90, 102636.
Vieira, T., Sandberg, U., Erlingsson, S., 2019. Negative texture, positive for the environment: effects of horizontal grinding of asphalt pavements. Road Mater. Pavement Des. 1–22.
Wang, X., Mohamed, Z., Ren, H., Liang, X., Shu, H., 2014. A study of tyre, cavity and rim coupling resonance induced noise. Int. J. Veh. Noise Vib. 10, 25–50.